Kinetics of C−NO and C−N2O reactions

ARTICLE *in* ENERGY & FUELS · OCTOBER 2001

Impact Factor: 2.79 · DOI: 10.1021/ef0001843

Articles

Kinetics of C−NO and C−N_2O Reactions

Sutee Wongtanakitcharoen,[†] Thanyarat Tatiyakiatisakun,[†] Thirasak Rirksomboon,[†] Richard Q. Long,[‡] Somchai Osuwan,[†] Pomthong Malakul,[†] and Ralph T. Yang*,[‡]

Petroleum and Petrochemical College, Chulalongkorn University, Bangkok, Thailand, and Department of Chemical Engineering, University of Michigan, Ann Arbor, Michigan 48109-2136

Received August 15, 2000. Revised Manuscript Received September 24, 2001

Apparent turnover frequency (TOF) rates for the C−NO reaction were calculated on the basis of overall rates measured for three graphite samples with different dimensions at various temperatures (500−750 °C) and partial pressures. These TOF rates were rates per edge site on the edges of the crystals. The TOF rates were also determined for one of these graphites for the C−N_2O reaction. Temperature breaks on the Arrhenius plots were observed for the C−NO reaction while no such temperature break was observed in TOF rates measured by directly following the etch pit growth rates (using STM). The temperature break phenomenon is attributed to pitting (and the ensuing pit growth) by O atoms dissociated from NO. The TOF rates appeared to be inversely proportional to the basal plane crystal size. This result was attributed to the steps and defects that also contributed significantly to the overall rates.

Introduction

The carbon gasification reactions, i.e., the reactions of C + O_2, C + CO_2, C + H_2O, C + H_2, and C + NO_x, have been studied extensively.[1−14] The importance of these reactions in combustion processes, catalysis, and metallurgy requires a fundamental understanding for these reactions. Among these reactions, the C + CO_2 reaction is the best understood one. The C + O_2, C + H_2O, and C + H_2 reactions are relatively well understood. The C + NO reaction is the least understood reaction. Many experimental techniques have been used in the studies of carbon gasification reactions. TPD (Temperature-Programmed Desorption), TGA (Thermogravimetric Analysis), and TK (Transient Kinetics) are among them. For single-crystal graphite, gold-decoration TEM (Transmission Electron Microscopy) was developed,[2,15] which allows one to investigate the gasification reactions taking place on the graphite basal plane through the formation of etch pits and channels by imaging the gold particles nucleated on the edges. A basic understanding of uncatalyzed and catalyzed carbon gasification has been obtained by the TEM technique.[16−23] More recently, STM (Scanning Tunneling Microscopy) was used to study the graphite basal plane reactions through surface topographic images,[24−27] which included monolayer etch pits and channeling.

The C + NO reaction is attracting wide interest because of its environmental ramifications. The emission of nitric oxides (NO and N_2O) from combustion processes is the cause for several environmental problems, including the formation of acid rain, stratospheric ozone depletion, and the "greenhouse" effect. Moreover,

* Corresponding author. Tel: +1-734-936-0771. Fax: +1-734-763-0459. E-mail: yang@umich.edu.
† Chulalongkorn University.
‡ University of Michigan.

(1) Walker, P. L., Jr.; Rusinko, F., Jr.; Austin, L. G. *Adv. Catal.* **1959**, *11*, 133.
(2) Yang, R. T. *Chem. Phys. Carbon* **1984**, *19*, 163.
(3) Laine, N. R.; Vastola, F. J.; Walker, P. L., Jr. *J. Phys. Chem.* **1963**, *67*, 2030.
(4) Radovic, L. R.; Jiang, H.; Lizzio, A. A. *Energy Fuels* **1991**, *5*, 68.
(5) Huttinger, K. L.; Nill, J. S. *Carbon* **1990**, *28*, 457.
(6) Chen, S. G.; Yang, R. T. *J. Catal.* **1993**, *141*, 102.
(7) Ergun, S.; Mentser, M. R. *Chem. Phys. Carbon* **1965**, *1*, 203.
(8) Walker, P. L., Jr.; Shelef, M.; Anderson, R. A. *Chem. Phys. Carbon* **1968**, *4*, 287.
(9) Baker, R. T. K. *Carbon and Coal Gasification Science and Technology*, NATO ASI Series E **1986**, *105*, 231.
(10) Floess, J. K.; Longwell, J. P.; Sarofim, A. F. *Energy Fuels* **1988**, *2*, 18.
(11) Kelemen, S. R.; Freund, H. *Carbon* **1975**, *23*, 619.
(12) Su, J. L.; Perlmutter, D. D. *AIChE J.* **1985**, *31*, 1725.
(13) McKee, D. W. *Adv. Catal.* **1981**, *16*, 1.
(14) Thomas, J. M. *Adv. Catal.* **1965**, *1*, 120.
(15) Hennig, G. R. *.Chem. Phys. Carbon.* **1966**, *2*, 1.
(16) Yang, R. T.; Wong, C. *Science* **1981**, *214*, 437.
(17) Yang, R. T.; Wong, C. *J. Chem. Phys.* **1981**, *75*, 4471.
(18) Yang, R. T.; Wong, C. *J. Catal.* **1984**, *85*, 154.
(19) Goethel, P. J.; Yang, R. T. *J. Catal.* **1986**, *101*, 342.
(20) Goethel, P. J.; Yang, R. T. *J. Catal.* **1987**, *108*, 356.
(21) Pan, Z.; Yang, R. T. *J. Catal.* **1990**, *123*, 206.
(22) Pan, Z.; Yang, R. T. *J. Catal.* **1991**, *130*, 161.
(23) Chen, S. G.; Yang, R. T. *J. Catal.* **1993**, *141*, 102.
(24) Chang, H.; Bard, A. J. *J. Am. Chem. Soc.* **1990**, *112*, 4598.
(25) Chu, X.; Schmidt, L. D. *Ind. Eng. Chem. Res.* **1993**, *32*, 1359.
(26) Chu, X.; Schmidt, L. D.; Chen, S. G.; Yang, R. T. *J. Catal.* **1993**, *140*, 543.
(27) Tandon, D.; Hippo, E. J.; Marsh, H.; Sebok, E. *Carbon* **1997**, *35*, 35.

10.1021/ef0001843 CCC: $20.00
Published on Web 10/23/2001

localized nitric oxides from energy generation power plants can cause respiratory system problems.[28,29] It was found that the use of carbon with proper catalysts to convert nitric oxides to CO_2 and N_2 in the combustion process is a possible approach for the reduction of nitrogen oxides.[30] However, the C + NO reaction is studied much less than the other carbon gasification reactions, and its understanding is in a primitive stage. There are no satisfactory kinetic models for the reaction, and much less is known about the reaction mechanism. Several groups have investigated the C + NO reaction.[31−52] There are a few excellent reviews for the C + NO reaction.[53,54] The general conclusions on the C + NO reaction are the following: (a) there is a very poor correlation between all available experimental kinetic data, and the situation is the same for even graphite samples, the highest ordered form of carbon; (b) there is a temperature "break" point in the Arrhenius plot (below about 650 °C), where the activation energy of the reaction increases from 15 to 30 kcal/mol in the lower temperature range to 40 kcal/mol in the higher temperature range; but at the same time, many investigators did not observe such a "break"; (c) it is a first-order reaction with respect to NO concentration; (d) graphite samples generally exhibited low reactivities and high activation energies, although a large range of activation energies was observed. Chu and Schmidt studied the intrinsic kinetics of the reactions between graphite and NO_x (i.e., NO, N_2O, and NO_2) by the STM technique, and important conclusions have been reached.[25,35] However, the highest temperature in their study was 650 °C, hence the important question on the temperature break could not be addressed.

Molecular orbital theory has been used to understand the mechanisms of gas−graphite reactions for about a decade.[55−62] Important insights have been gained for both uncatalyzed and catalyzed reactions by molecular orbital studies.

More recently, Yang and co-workers measured the intrinsic kinetics of the C + NO_x reactions in the temperature range 500−900 °C, using the STM technique.[63] Turnover frequency (TOF) rates were measured from the etch-pit growth rates on the basal plane of graphite. From the TOF rates, no temperature break was observed. At temperatures above 700 °C, at NO partial pressures over 0.01 atm, many new etch pits that originated from new vacancies generated from O atoms were formed. Moreover, deep pits began to form at still higher temperatures and concentrations, again, due to O atoms. The O atoms were attributed to the dissociation of NO/N_2O. In this work, we measured TOF rates, using TGA, on graphite crystals with different dimensions. The results will be used to understand the crystal-size dependence of TOF and also to further understand the temperature break phenomenon.

Table 1. Dimensions of Graphite Samples

graphite	avg. diameter μm	avg. thickness μm	surface area m^2/g
SP-1	33	0.46	2.01
Micro-450	5	0.05	22.9
Micro-850	3.5	0.06	12.9

Experimental Section

Graphite Samples, Gases, and Gas Purification. Three graphites with relatively uniform dimensions were used. They were SP-1, Micro-450, and Micro-850. The SP-1 graphite was obtained from Union Carbide Carbon Products Division. The other two graphites were obtained from Asbury Graphite Mills. All three graphites were highly graphitic, of high purity, and were of uniform disk-shaped sizes. Their dimensions are given in Table 1, along with their surface areas. The impurities in the three samples were <100 ppm (SP-1), 0.66% (Micro-450), and 0.56% (Micro-850).

The nitric oxide (NO) used for the gasification reaction had a purity of 99.5% and was supplied by Intergas Co., Ltd. (Thailand). The nitrous oxide (N_2O) used for gasification reaction was of 99.5% purity. The helium used as diluent and carrier gas for gas chromatographs (GC) was of an ultrahigh purity of 99.999%. The two latter gases were obtained from Thai Industrial Gases Public Co., Ltd. Moisture and oxygen impurities in the He gas were further removed by a moisture trap and an oxygen trap, respectively.

The flow rates of each stream were controlled by Side-Trak Model 840 mass flow controllers. Either NO or N_2O was blended with He in a mixing chamber to obtain the desired concentration. Next, any trace of residual oxygen was removed by an oxygen removal unit. This unit contained a packed bed of copper flakes and was maintained at 550 °C. To ensure that the residual oxygen was removed, the oxygen concentration was analyzed by GC.

Determination of Turnover Frequency Rates. Thermogravimetric analysis (TGA) was used to measure the weight loss rates. A Du Pont Model 2950 thermogravimetric analyzer

(28) Hayhurst, A. N.; Lawrence, A. D. *Combust. Sci.* **1992**, *18*, 529.
(29) Wojtowicz, M. A.; Pels, J. R.; Moulijn, J. A. *Fuel Process. Technol.* **1993**, *34*, 1.
(30) Ruckenstein, E.; Hu, Y. H. *Ind. Eng. Chem. Res.* **1997**, *36*, 2533.
(31) Chambrion, P.; Suzuki, T.; Zhang, Z.; Kyotani, T.; Tomita, A. *Energy Fuels* **1997**, *11*, 681.
(32) Garcia-Garcia, A.; Chinchon-Yepes, S.; Linares-Solano, A.; Salinas-Martinez de Lecea, C. *Energy Fuels* **1997**, *11*, 292.
(33) Shakti, G.; Zhang, B.; Sarofim, A. F. *Combust. Flame* **1996**, *104*, 213.
(34) DeGroot, W. F.; Richards, G. N. *Carbon* **1991**, *29*, 179.
(35) Chu, X.; Schmidt, L. D. *Surf. Sci.* **1992**, *268*, 325.
(36) Teng, H.; Suuberg, Eric M. *Ind. Eng. Chem. Res.* **1993**, *32*, 416.
(37) Zhu, Z. H.; Radovic, L. R.; Lu, G. Q. *Carbon* **2000**, *38*, 451.
(38) Chen, W.; Ma, L. *AIChE J.* **1996**, *42* (2), 1968.
(39) Teng, H.; Lin, H.; Hsieh, Y. *Ind. Eng. Chem. Res.* **1997**, *36*, 524.
(40) Teng, H.; Lin, H. *Carbon* **1997**, *35*, 1811.
(41) Lee, S.; Permana, H.; Ng, K. Y. S. *Carbon* **1994**, *32*, 145.
(42) Levy, J. M.; Chan, L. K.; Sarofim, A. F.; Beer, J. M. *Eighteenth Symp. Combust.* **1981**, 111.
(43) Teng, H.; Suuberg, E. M.; Calo, J. M. *Energy Fuels* **1992**, *6*, 398.
(44) Teng, H.; Suuberg, E. M. *J. Phys. Chem.* **1993**, *97*, 478.
(45) Illan-Gomez, M. J.; Linares-Solano, A.; Salinas-Martinez de Lecea, C. *Energy Fuels* **1993**, *7*, 146.
(46) Illan-Gomez, M. J.; Linares-Solano, A.; Radovic, L. R.; Salinas-Martinez de Lecea, C. *Energy Fuels* **1996**, *10*, 158.
(47) Suzuki, T.; Kyotani, T.; Tomita, A. *Ind. Eng. Chem. Res.* **1994**, *33*, 2840.
(48) Yamashita, H.; Tomita, A. *Energy Fuels* **1993**, *7*, 85.
(49) Richthofen, A. V.; Wendel, E.; Neuschutz, D. *Fresenius J. Anal. Chem.* **1993**, *346*, 261.
(50) Jang, B. L.; Spivey, J. J.; Kung, M. C.; Kung, H. H. *Energy Fuels* **1997**, *11*, 299.
(51) Marquez-Alvarez, C.; Rodriguez-Ramos, I.; Guerrero-Ruiz, A. *Carbon* **1996**, *34*, 1509.
(52) Miettinen, H.; Abul-Milh, M. *Energy Fuels* **1996**, *10*, 421.
(53) Aarna, I.; Suuberg, E. M. *Fuel* **1997**, *76*, 475.
(54) Li, Y. H.; Lu, G. Q.; Rudolph, V. *Chem. Eng. Sci.* **1998**, *53*, 1.
(55) Pan, Z.; Yang, R. T. *J. Catal.* **1990**, *123*, 206.
(56) Pan, Z.; Yang, R. T. *Ind. Eng. Chem. Res.* **1992**, *31*, 2675.
(57) Chen, S. G.; Yang, R. T. *J. Catal.* **1993**, *141*, 102.
(58) Kyotani, T.; Tomita, A.; Radovic, L. R. *AIChE J.* **1996**, *42*, 2303.
(59) Chen, S. G.; Yang, R. T. *Energy Fuels* **1997**, *11*, 1, 421.
(60) Chen, N.; Yang, R. T. *Carbon* **1998**, *36* (6), 1061.
(61) Chen, N.; Yang, R. T. *J. Phys. Chem. A* **1998**, *102*, 6348.
(62) Kyotani, T.; Tomita, A. *J. Phys. Chem. B* **1999**, *103*, 3434.
(63) Chen, N.; Yang, R. T.; Goldman, R. S. *J. Catal.* **1998**, *180*, 245.

with a nominal sensitivity of 0.1 μg was employed. To avoid or minimize interparticle mass transfer resistance, typically 5 mg of sample was used in the carbon−nitric oxide reaction and 7 mg was used for the carbon−nitrous oxide reaction. These amounts were determined empirically.

Prior to each run, the graphite sample was degassed at 120 °C in He for 2 h in order to remove the physically adsorbed gases and to clean the surface. A flow distribution of helium was set at 40 and 60 mL/min in the balance chamber and furnace chamber purge, respectively. After degassing and surface cleaning, the sample was heated to the desired reaction temperature with a ramp rate of 10 °C/min in a He flow. When the desired reaction temperature was reached, NO or N_2O gas at a desired concentration was switched instead of He and passed through the TGA reactor with a flow rate of 60 mL/min to react with the degassed sample. During the reaction, the product gases were continuously analyzed by GC. After a certain time of reaction, the reaction gases were switched back to helium and the temperature was allowed to drop to ambient temperature quickly in order to reduce any postreaction.

Because the edge sites on the graphite samples were active sites, the gasification rates of graphite in NO or N_2O could be determined in terms of the rate per active site or TOF. However, it should be noted that the TOF rates presented in this work were based on the average crystal dimensions (Table 1) assuming perfect crystals with no edge sites on the flat faces. Hence these are apparent TOF rates. The graphite gasification by NO or N_2O was studied under isothermal conditions. Both these reactions were studied at temperatures from 500 °C to 750 °C, at NO concentrations of 6%, 20%, 40%, and at N_2O concentrations of 6%, 12%, 20%. The total flow rate of gases passing through the TGA reactor was maintained at 100 mL/min. These conditions were empirically determined under which mass transfer resistances were eliminated, hence enabling determination of the intrinsic rates. Because the reaction rate changed to some extent at both very low and very high burnoff levels, only reaction rates between 10% and 20% burnoff were used. The apparent TOF rates were measured both as a function of reaction temperature and as a function of NO or N_2O concentration.

The turnover frequency, as the rate per active or edge site, was obtained, following Yang and Wong,[2,17] as

$$\mathrm{TOF}\left(\frac{\text{atoms gasified}}{\text{edge atom/s}}\right) = \frac{\text{atoms gasified/time}}{\rho_{11\bar{2}0} A_2} \qquad (1)$$

where $\rho_{11\bar{2}0}$ is the number of active sites per edge surface area (= 0.120 carbon atoms/A^2) and A_2 is the edge surface area of the graphite.

Results and Discussion

Graphite−Nitric Oxide Reaction. As discussed above, the turnover frequency (TOF) rates were measured at different temperatures and partial pressures for the three graphites. As mentioned, these TOF rates were based on the edge surfaces, not including the sites on the flat surfaces. The rates in the range of 10−20% burnoff were quite steady and were used to calculate all TOF data in this work. Typical results are shown for the Micro-850 graphite, in Figure 1. The reaction temperature and NO concentration dependence of TOF can be expressed by

$$\mathrm{TOF} = A_0 P_{\mathrm{NO}}^{n} e^{-E_a/RT} \qquad (2)$$

where A_0 is the preexponential factor, n is the reaction order with respect to NO partial pressure, P_{NO} is the NO partial pressure, E_a is the activation energy, R is the gas constant, and T is the temperature. The dependence on partial pressure is further expressed by

$$\ln \mathrm{TOF} = \ln k + n \ln P_{\mathrm{NO}} \qquad (3)$$

Using this expression, the pressure dependence is seen in Figure 2. This plot indicates that the reaction is approximately first-order with respect to NO. First-order was also reported in all previous literature for this reaction.[53,54]

The activation energy can be determined from the Arrhenius plot, which is shown in Figure 3 for 6% NO. A temperature break is clearly seen in this plot. The apparent activation energies for the two temperature regimes (i.e., below and above the temperature break point) are given in Table 2. The activation energies for all three graphites are also included in this table, along with the values from the literature data.

Graphite−Nitrous Oxide Reaction. Similar to the C−NO reaction, the apparent TOF rates were measured for one of the three graphites, Micro-850, at various temperatures and partial pressures. The effects of reaction temperature and N_2O concentration at 6%, 12%, and 20% N_2O are shown in Figure 4. The activation energy can be determined from the Arrhenius plot, shown in Figure 5 for 6%, 12%, and 20% N_2O concentrations. It is apparent that a temperature break did

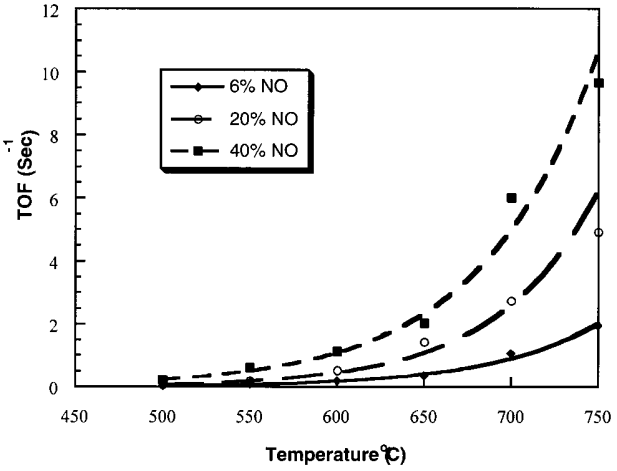

Figure 1. Apparent turnover frequency (TOF) rates (based on edge areas of the crystals) for the reaction between NO and Micro-850 graphite at different temperatures and partial pressures.

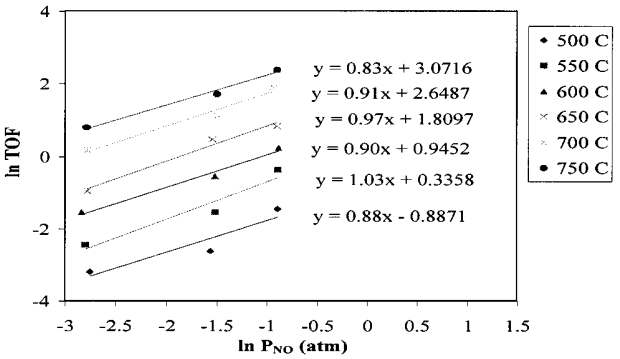

Figure 2. Correlations between NO partial pressure and apparent TOF for NO reaction with Micro-850 graphite in the temperature range of 500−750 °C.

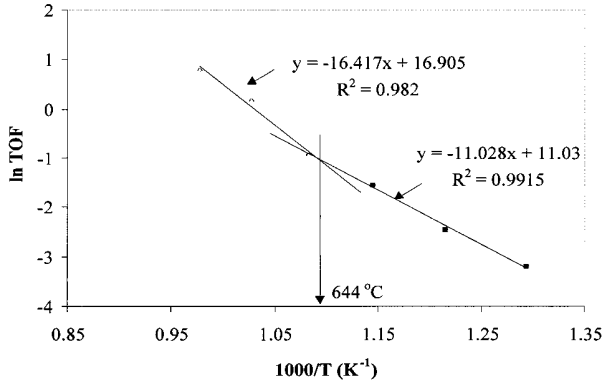

Figure 3. Arrhenius plot of the reaction for NO−Micro-850 graphite at 6% NO concentration (0.06 atm).

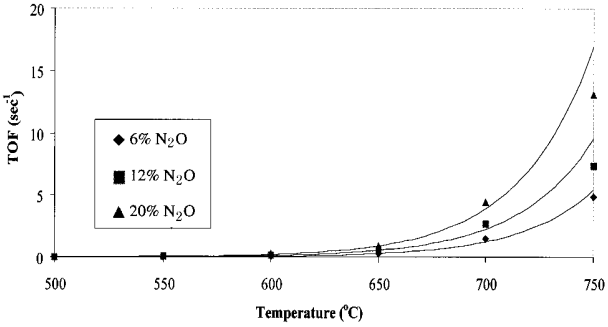

Figure 4. Effect of reaction temperature and N_2O concentration on apparent TOF for N_2O reaction with Micro-850 graphite at (from the top): 20%, 12%, and 6% N_2O.

Table 2. Comparison of Activation Energies of the Carbon−NO Reaction for SP-1, Micro-450, and Micro-850 Graphites with Literature Data[53]

				E_a (kJ/mol)	
carbon type	reactor	temperature range (K)	P_{NO} (kPa)	low temp	high temp
Graphite	fixed bed	873−1173	0.04−0.0.90		239
Graphite	fixed bed	973−1223	0.05−0.15		162.7
Graphite	TGA	873−1223	1.0−8.1	65	200
Graphon	fixed bed	1027−1233	0.27−0.75		86.6
Graphite	fixed bed	950−1250	0.1−0.15		240
PF-char	TGA	723−1173	1.0−8.1	35	140
PF-char	TGA	773−1073	1.0−10.1	63−88	180
Micro 450	TGA	773−1073	6.0	64	110
Micro 450	TGA	773−1073	20.0		88
Micro 450	TGA	773−1073	40.0		80
SP-1	TGA	773−1073	6.0	84	122
SP-1	TGA	773−1073	20.0		93
SP-1	TGA	773−1073	40.0		83
Micro 850	TGA	773−1073	6.0	92	136
Micro 850	TGA	773−1073	20.0		116
Micro 850	TGA	773−1073	40.0		100
Activated carbon	fixed bed	773−1118	0.03−0.20	63.5	181
Cellulose char	TGA	773−923	10.1		64
Coconut char	TGA	673−1173	1.0−8.1	42	120

not occur in these temperature and pressure ranges. Teng et al.[39,40] studied the global kinetics of the carbon gasification in N_2O by a thermogravimetric system. A temperature break at 748 K was reported. Hence it is possible that the temperature range that was used in this work was not low enough to reach the break point, since the lowest temperature was 773 K.

The activation energies are listed in Table 3. The values (192−204 kJ/mol) are relatively high compared with the data reported in the literature (which fall in the wide range of 66−284 kJ/mol).[40] Similar to the reaction with NO, the reaction order with respect to NO partial pressure was approximately first-order, shown in Figure 6.

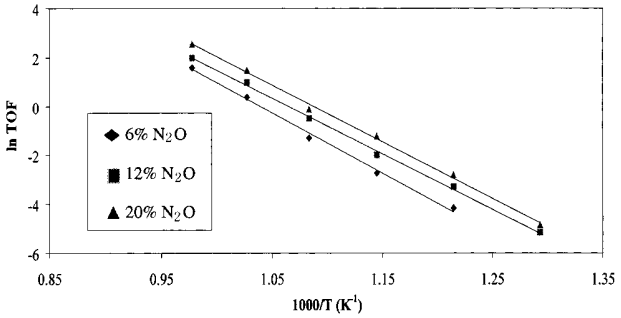

Figure 5. Arrhenius plot of apparent TOF rates for reaction of Micro-850 graphite with N_2O at (from the top) 20%, 12%, and 6% concentration (at 1 atm).

SEM Observation of the Basal Plane. The basal planes of unreacted and reacted SP-1 graphite crystals were studied by scanning electron microscopy (SEM). The unreacted basal plane is shown in Figure 7. The basal plane was essentially flat and featureless. However, some steps and ledges were clearly visible. After reaction with NO (6%) at 500 °C for 10 h, features began to develop, as seen in Figure 8. Here large steps, ledges, and islands were formed by gasification, mostly by edge recession. An SP-1 sample was then subjected to NO oxidation (6%) at 700 °C for 3 h, with 17% burnoff. The SEM picture of the reacted sample is shown in Figure 9. Another picture at a higher magnification is shown in Figure 10. Pitting became the main mode of reaction at 700 °C. Deep, conical shaped pits were abundant on the basal plane. The vigorous pitting clearly had a very significant contribution to the overall rates. The TOF rates that were calculated on the basis of the overall rates were therefore inflated. As explained previously by Yang et al.,[63] these pits were formed by O atoms because the dissociation constant of NO into O atoms is much higher than that of dissociation of O_2, H_2O, and CO_2 and that basal plane attack by O atoms could take place at low temperatures. A comparison of the dissociation constants is given in Table 4 and in ref 63.

The SEM observation will be important in understanding the unique temperature break phenomenon for the C−NO reaction, as well as the crystal size effect on the apparent TOF rates.

The Inverse Dependence of Kinetics on Crystal Diameter for the C−NO Reaction. The TOF rates for the C−NO reaction for the three graphites with different dimensions are compared in Figure 11. The TOF rates that were measured by Yang and co-workers[63] from etch pit growth rates of monolayer pits on the basal plane are also included for comparison.

The most important conclusion to be reached from this comparison is that the apparent TOF rates are approximately inversely proportional to the crystal diameter of the graphite. This result has significant inference on the kinetics of the C−NO reaction.

The TOF rates calculated in this work were based on the edge surfaces of the crystals (assuming disk shape). Any contributions from the basal planes (i.e., the two flat surfaces of the samples) were not included. The result that crystals with large diameters yielded higher

Table 3. Comparison of Kinetic Parameters of the N_2O−Carbon Reaction Using Micro-850 Graphite with Literature[39,40]

carbon type	reactor	temperature range (K)	N_2O pressure (kPa)	E_a (kJ/mol)	reaction order
Charcoal	static reaction	551−653	1−52	134	1
Charcoal	circulated batch	673−873	0.26−46	176	1
Graphon	circulated batch	673−923	0.17−50	284	1
Cedar Grove bit. Char	fixed bed	700−1250	0.008	116	
Prosper bit. Char	fixed bed	700−1250	0.008	101	
Eschweiler bit. Char	fixed bed	700−1250	0.008	83.1	
Norit RX act. Carbon	packed bed	640−720	0.0035−0.0045	96 ± 13	
DE53 lignite char	fixed bed	673−1223	0.019−0.19	77 ± 23	0.59 ± 0.4
Gardanne subbit. Char	fixed bed	673−1223	0.019−0.19	68 ± 27	0.58 ± 0.6
Daw-Mill bit. Char	fixed bed	673−1223	0.019−0.19	77 ± 17	0.59 ± 0.3
Blanzy anthr. Char	fixed bed	673−1223	0.019−0.19	66 ± 9	0.61 ± 0.2
Norit RX act. Carbon	fixed bed	673−1223	0.019−0.19	77 ± 23	0.59 ± 0.4
Micro850	TGA	773−1073	6.0	204	1
Micro 850	TGA	773−1023	12.0	196	1
Micro850	TGA	773−1023	20.0	192	1

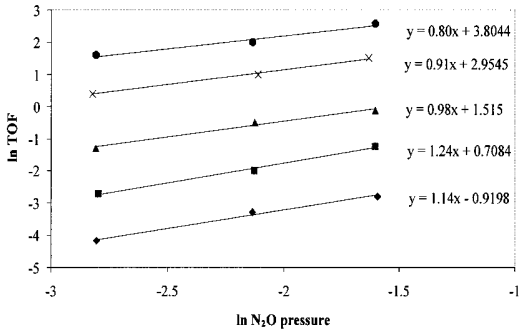

Figure 6. Correlation between N_2O partial pressure and apparent TOF for N_2O reduction with Micro-850 graphite at different temperatures (from the top): 750, 700, 650, 600, and 550 °C.

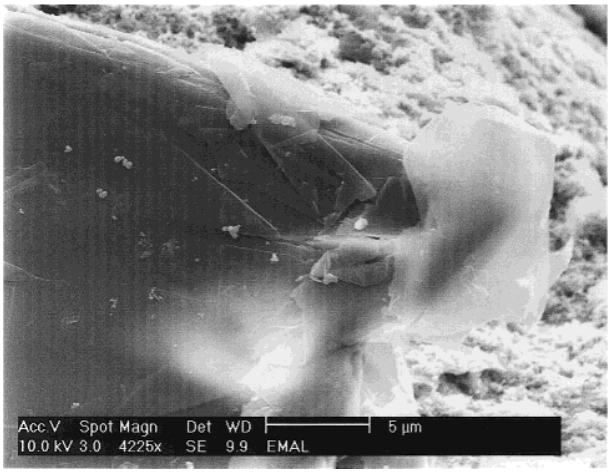

Figure 7. SEM picture of the unreacted basal plane of SP-1 graphite.

TOF rates indicate that the basal plane has a significant contribution toward the calculated TOF rates. Crystals with larger diameters would have larger basal planes per edge site. Hence it appears that the contribution from the basal plane for gasification is due to edge recession on the steps and ledges at low temperatures (i.e., below the temperature break point) as well as pitting by O atoms at higher temperatures. Therefore, the TOF rates calculated on the basis of the edge sites (without considering the basal plane contribution) would be higher for crystals with larger diameters (which have higher basal plane area/edge site).

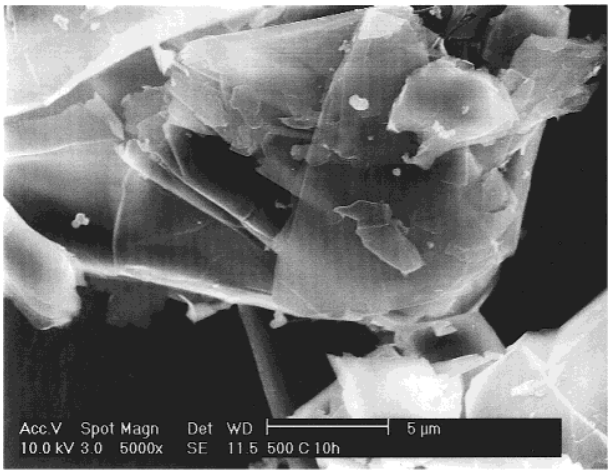

Figure 8. SEM picture of the basal plane of SP-1 graphite after reaction with 6% NO at 500 °C for 10 h.

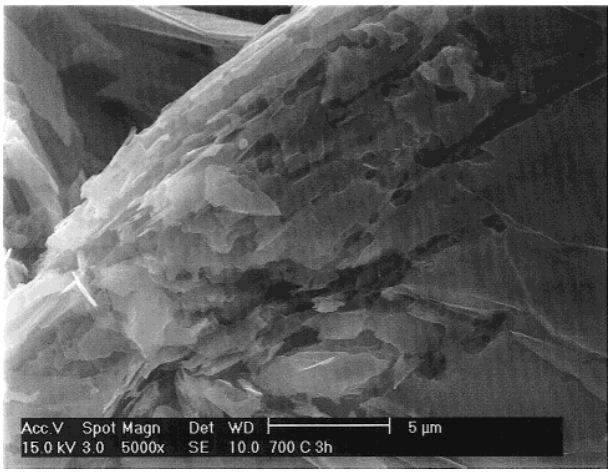

Figure 9. SEM picture of the basal plane of SP-1 graphite after reaction with 6% NO at 700 °C for 3 h.

It would be extremely difficult to quantitatively characterize the contribution from the new pits formed on the basal plane. However, from Figure 11, this contribution increased as the temperature was increased (since Figure 11 is a semilog plot).

Temperature Break Phenomenon. Temperature break was indeed observed for the TOF rates of the C−NO reaction on single-crystal graphites. Our earlier study by monolayer etch pit growth on the basal plane

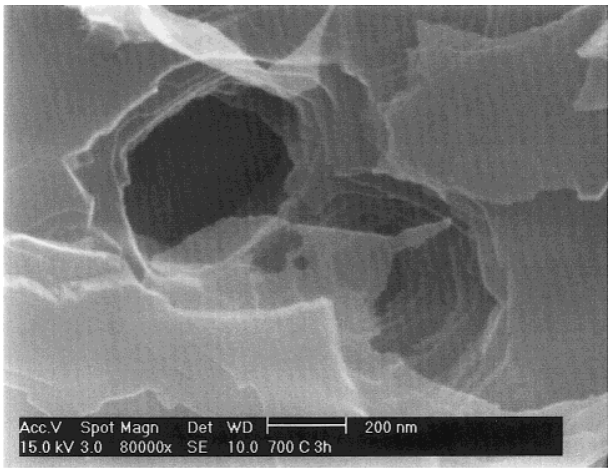

Figure 10. SEM picture of the basal plane of SP-1 graphite after reaction with 6% NO at 700 °C for 3 h.

Table 4. Comparison of Homogeneous Dissociation Constants (*K*)

	$K^{a,b}$			
T (°C)	NO → O + N	2NO → N_2O + O	N_2O → N_2 + O	O_2 → O + O
925	1.9×10^{-22}	3.2×10^{-9}	3.6×10^{-8}	6.2×10^{-16}
825	5.7×10^{-25}	7.7×10^{-10}	1.6×10^{-8}	6.1×10^{-18}
725	5.3×10^{-28}	1.4×10^{-10}	6.7×10^{-9}	2.4×10^{-20}
625	1.0×10^{-31}	1.8×10^{-11}	2.2×10^{-9}	2.8×10^{-23}
525	2.5×10^{-36}	1.3×10^{-12}	5.6×10^{-10}	6.2×10^{-27}
425	2.8×10^{-42}	5.0×10^{-14}	1.8×10^{-10}	1.3×10^{-31}

[a] Calculated from free energies of formation data, *JANAF Thermochemical Tables*, 2nd ed., NSRDS, National Bureau of Standards, Washington, D.C., 1971. [b] The dissociation constants for CO_2 and H_2O are given in ref 63.

showed no temperature break for this reaction in the entire temperature range of 500−900 °C,[63] also shown in Figure 11. With 1% NO, starting at about 700 °C, new pit formation occurs on the basal plane.[63] At >800 °C, deep pits were formed vigorously at 1% NO.[63] We have attributed the temperature break phenomenon as the result of the nascent pits formation and the deep pits formation at high temperatures. The O atom concentration is substantially higher in NO than in O_2, CO_2, and H_2O, due to the substantially higher equilibrium dissociation constants of NO (Table 4 and ref 63). Hence, we have attributed the temperature break as the result of pitting by O atoms. This reasoning is substantiated by the SEM observations, shown in Figures 7−10.

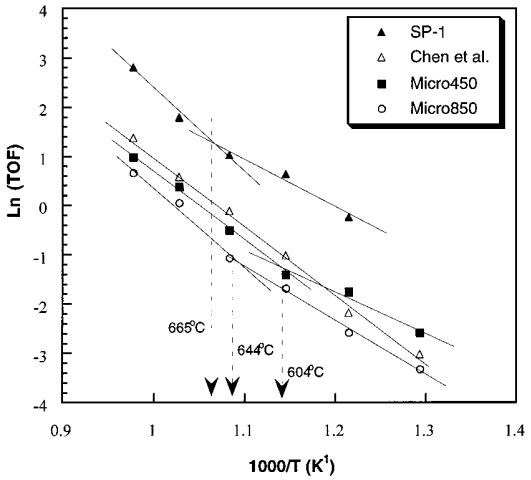

Figure 11. Apparent TOF rates (atom/atom/s) for the graphite−NO reaction (at 0.06 atm NO) for graphites with different dimensions (see Table 1). The data by Chen et al.[63] were measured by monolayer etch pit growth rates on the basal plane using STM at 0.05 atm NO but converted into 0.06 atm via first-order dependence.

At 6% NO, vigorous, deep pitting took place at 700 °C, shown in Figures 9 and 10.

At 6% NO, the temperature break occurs between 600 and 665 °C for the three graphites under study. At 20% and 40%, the temperature break is expected to be lower, and apparently they have been missed in our experiments which started at 500 °C.

For the C−N_2O reaction, temperature break was not observed within the temperature range studied. Since the dissociation constant for N_2O is higher than that of NO by approximately 2 orders of magnitude (Table 4), the temperature break point was apparently lower than the lowest temperature in the study, i.e., 500 °C.

The apparent TOF on the SP-1 graphite are higher than the two other even at *T* below the break point. This indicates a substantial amount of contribution from the basal plane at 6% NO. This is attributed to the edge recession that took place on the basal plane.

Acknowledgment. Support from NSF under CTS-9523801 is gratefully acknowledged. We are also grateful to Dr. Albert Tamashausky of Asbury Graphite Mills for discussion and the samples.

EF0001843